


 Cite this: *Lab Chip*, 2019, 19, 618

# A microfluidic platform integrated with field-effect transistors for enumeration of circulating tumor cells†‡

 Yi-Hong Chen,<sup>a</sup> Anil Kumar Pulikkathodi,<sup>b</sup> Yu-Dong Ma,<sup>a</sup>  
Yu-Lin Wang <sup>\*ab</sup> and Gwo-Bin Lee <sup>\*abc</sup>

Circulating tumor cells (CTCs) are one of the promising cancer biomarkers whose concentrations are measured not only in the initial diagnostic stages, but also as treatment progresses. However, the existing methods for CTC detection are relatively time-consuming and labor-intensive. In this study, a new microfluidic platform integrated with field-effect transistors (FETs) and chambers for the trapping of CTCs was developed. This novel design could not only trap CTCs from whole blood samples, but also enumerate them *via* FET sensing of CTC-specific aptamer–CTC complexes. The FET output signal was experimentally found to increase with the increasing number of captured CTCs. More importantly, the enumeration of spiked CTCs in blood samples could be achieved in accordance with the signals measured on the FET devices. We therefore believe that this automated system could be a useful tool for enumeration of CTCs.

 Received 9th October 2018,  
Accepted 4th January 2019

DOI: 10.1039/c8lc01072b

rsc.li/loc

## Introduction

Cancer is among the leading causes of non-accident-related deaths across the globe. According to the World Health Organization, 12 million new cancer cases are diagnosed every year, and approximately 9 million deaths a year are attributed to cancer, making it the second leading cause of death worldwide.<sup>1</sup> For instance, in 2015 one out of six deaths was caused by cancer. Early diagnosis can increase the odds of survival significantly; there is consequently an urgent need to develop early-warning biomarkers for a variety of different cancer types.

Recently, detection of circulating tumor cells (CTCs) in liquid biopsies has been shown to be a promising method for early-cancer diagnosis.<sup>2</sup> CTCs were discovered a century ago, and scientists have 1) investigated the mechanisms of metastasis and 2) recognized the relationship between CTCs and the spread of carcinomas.<sup>3</sup> Generally speaking, CTCs are

tumor cells with extraordinary mobility, which allows them to transit throughout the circulatory system and invade other tissues. Secondary tumors may then spread to and then grow in other organs *via* blood circulation of CTCs; these cells consequently contribute significantly to the lethal nature of many cancers.

For these reasons, detection of CTCs as early as possible is critical. In fact, CTCs may be measured in human blood before traditional tissue biopsies show signs of cancer.<sup>4</sup> Quantification of CTC concentration is also useful for evaluating the efficacy of therapy; they could therefore serve as biomarkers not only for cancer diagnosis, but also for patient prognosis after therapy. Early detection and frequent monitoring of cancer are both associated with the higher patient survival rate.<sup>5</sup> However, CTCs are normally documented at low concentrations (~one for every million white blood cells (WBCs)) and are consequently difficult to detect in human blood samples.<sup>6,7</sup> Normally, then CTC enrichment steps are taken prior to detection.<sup>8</sup>

Recently, microfluidic systems have been used in a wide variety of biological applications,<sup>9–12</sup> including CTC enrichment. For instance, microstructural filters were used to concentrate CTCs to detectable levels,<sup>13</sup> and this method has shown great potential in the clinic.<sup>14–16</sup> Additionally, deterministic lateral displacement (DLD) was developed to isolate CTCs by using the differentiation of the cell size with a laminar flow<sup>17</sup> with a separation efficiency of up to 85%.<sup>18</sup> Furthermore, several approaches have emerged recently for CTC isolation. For instance, a platform to isolate cancer cells from whole blood with shear-induced diffusion was

<sup>a</sup> Department of Power Mechanical Engineering, National Tsing Hua University, Hsinchu, Taiwan 30013. E-mail: gwobin@pme.nthu.edu.tw; Tel: +886 3 5715131 Ext. 33765

<sup>b</sup> Institute of Nano-Engineering and Microsystems, National Tsing Hua University, Hsinchu, Taiwan 30013. E-mail: yhwang@mx.nthu.edu.tw; Tel: +886 3 5715131 Ext. 80159

<sup>c</sup> Institute of Biomedical Engineering, National Tsing Hua University, Hsinchu, Taiwan 30013

† The preliminary results of the current study were presented at the 21st International Conference on Miniaturized Systems for Chemistry and Life Sciences (MicroTAS 2017) in Savannah, Georgia (USA), Oct. 22–26, 2017.

‡ Electronic supplementary information (ESI) available. See DOI: 10.1039/c8lc01072b

reported, resulting in a high separation efficiency (89.8%) at a throughput of  $6.75 \text{ mL h}^{-1}$  ( $10^6$ – $10^7$  cells per s).<sup>19</sup> Alternatively, hydrodynamic trapping has been used to effectively trap and collect small particles or cells on microfluidic platforms.<sup>20–22</sup> Moreover, a microfluidic device capable of size-selective cell separation from diluted blood samples and highly efficient entrapment of single cells was demonstrated.<sup>23,24</sup> The basic principle of hydrodynamic trapping is to use narrow side-channels with a lower flow resistance such that the main stream of the liquid leaves the particles/cells trapped, providing a higher likelihood of achieving continuous cell trapping and retrieval thereafter.<sup>25–27</sup>

Immunofluorescence labeling methods have been commonly applied for detecting and imaging CTCs, as they overcome, to some extent, low specificity issues inherent to microstructural trapping methods.<sup>4</sup> However, they are relatively laborious and require well-trained personnel.<sup>28–31</sup> Electronic sensors have also been demonstrated to detect CTCs.<sup>32,33</sup> For instance, field-effect transistors (FETs) can be applied as biosensors for cell detection due to their high transconductance gain.<sup>34</sup> Among them, aluminum gallium nitride/gallium nitride (AlGaN/GaN) high electron mobility transistors can quickly detect deoxyribonucleic acid (DNA) and cells with high sensitivity over a wide dynamic range.<sup>34</sup> When compared with conventional CTC detection devices, they are compact, label-free, and sensitive and provide exact cell count data.

One challenge with using FETs as biosensors is the need to immobilize affinity reagents on the open gate of the FETs; these probes are vital for cell identification. Generally speaking, antibodies specific to surface antigens of cell membranes have been commonly used for this purpose, though aptamers, which are highly specific probes that can bind target molecules or even cells,<sup>35,36</sup> have been used instead more recently. When compared to commercial antibodies, aptamers not only have comparable, or even superior, affinity and specificity, but are also cheaper, more stable, and easier to synthesize (leading to essentially zero batch-to-batch variation).<sup>37–39</sup> Additionally, specific probes or dyes can be easily conjugated to aptamers during their chemical synthesis, which makes them readily customizable affinity reagents. Given these attributes, we hypothesized herein that we could develop an automated microfluidic platform integrated with 1) CTC-specific aptamer-bound FET sensor arrays and 2) cell trapping devices capable of both detecting and enumerating CTCs. Cancer cell specific aptamers were immobilized on top of FETs to specifically recognize cancer cells. Additionally, hydrodynamic microstructures (*i.e.* cell trapping devices) provide efficient and continuous trapping of cancer cells. Furthermore, the FET sensor array was used to detect and count trapped cancer cells, in a physiological concentration ( $\sim 150 \text{ mM NaCl}$ ), without performing additional sample processing. The entire process could be automated on the integrated microfluidic chip. It is the first time that an integrated microfluidic chip equipped with FET sensor arrays immobilized with CTC-specific aptamers has been demonstrated, enabling the continuous trapping of CTCs and enumeration thereafter.

Furthermore, the captured CTCs could be retrieved afterwards for subsequent applications (such as culture and analysis). Therefore, it could be an amenable and useful tool for CTC applications.

## Experimental

After red blood cell (RBC) lysis and WBC depletion, CTCs were isolated with magnetic beads surface-coated with cancer cell-specific aptamers and transported into the integrated microfluidic chip composed of cell trapping chambers and embedded FET sensor arrays (Fig. 1). The microchannels were designed such that CTCs could be trapped hydrodynamically on top of each FET sensor aligned with these cell-trapping devices. Finally, the current gain of the FET sensors was measured to serve as a proxy for the target cancer cell number. Each step discussed in this paragraph is explained in detail below.

### Chip fabrication

To fabricate the microfluidic chip, an SU-8 standard lithography technique was first used to form the microstructure master mold.<sup>27</sup> Briefly, a  $30 \mu\text{m}$ -thick layer of SU-8 3035 (MicroChem, USA) was spin-coated on a silicon wafer with a spin-coater (M&R Nano Technology, Taiwan). After a 12 min soft-baking process, the SU-8 microstructures were formed at a dosage of  $166 \text{ mJ cm}^{-2}$  by a standard lithography process. After another

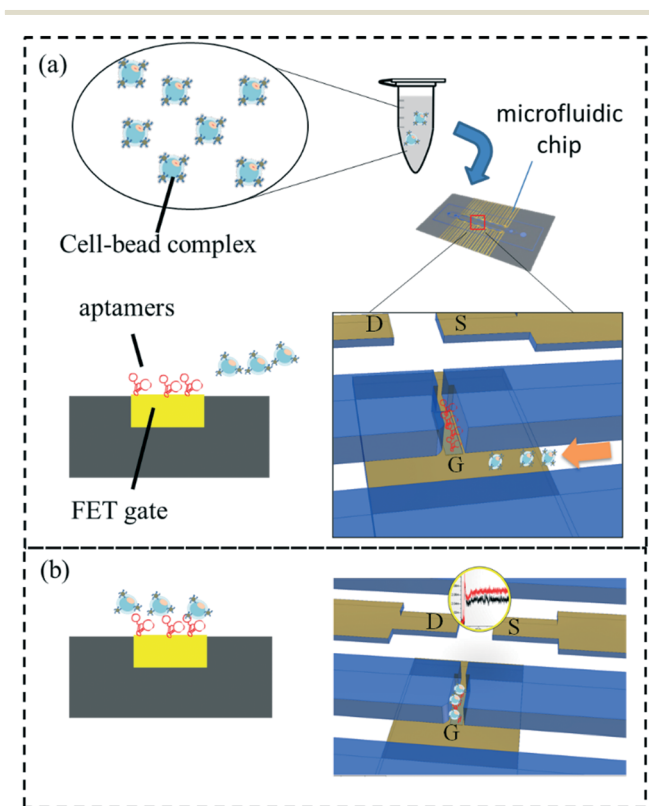
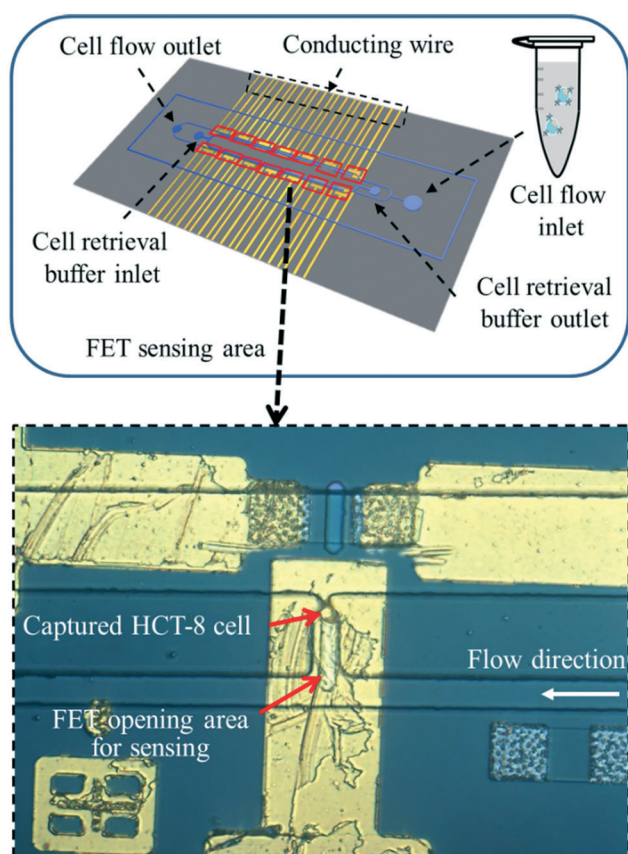


Fig. 1 A schematic illustration of the CTC capture and detection processes: (a) sample injection; (b) CTC trapping and FET sensing. D = drain, S = source, and G = gate.

post-exposure bake (65 °C for 1 min and 95 °C for 5 min) and a standard SU-8 developing process, the master mold featuring the microstructures was formed. Afterwards, a polydimethylsiloxane (PDMS, Sylgard184A/B, Dow Corning, USA) soft lithography technique was used to replicate microfluidic structures with inverse microstructures on the master mold.<sup>40</sup> Briefly, two PDMS reagents were mixed at a weight ratio of 10 : 1, poured into the SU-8 master mold, and then baked at 80 °C for 30 min. Then, the cured, inverse microstructures of PDMS were mechanically de-molded from the master mold, and the inlets and outlets of the microfluidic chip were created with biopsy punch needles (Miltex, USA). Detailed information about the fabrication of the microfluidic device can be found in Fig. S1.† The microfluidic chip was then equipped with FET sensors using the process described below.

### Chip design

The upper layer of the integrated, dual-layer microfluidic device (Fig. 2) was composed of a microfluidic chip with two inlets (for injection of cells and phosphate buffered saline (PBS; the wash buffer) and 14 individual trapping chambers (60 × 20 × 30 μm; length × width × height) distributed equally



**Fig. 2** A schematic illustration of the integrated microfluidic system, which was composed of a microfluidic chip and an FET-sensor-array-embedded epoxy substrate capable of capturing cancer cells on the FET sensing area.

across two parallel microchannels (2 × 7 array (Fig. 3a)). Cells were hydrodynamically carried into the cell traps by the main fluid stream and then trapped by the channels' narrow necks (width = 5 μm) due to the lower flow resistance in the trapping channel (Fig. 3b). Each chamber could trap up to three CTCs with diameters of ~20 μm. Once the cells partially obstructed the gap and decreased the fracture of the streamline, the traps became sealed (impermeable to additional cells); the ensuing cells then moved to the next (downstream) trapping chamber.

The bottom layer of the device was the FET sensor array embedded on an epoxy substrate (Fig. 4a). FET sensors can rapidly detect signals with high accuracy and precision, even in solutions with high ion concentrations (*e.g.*, PBS or culture media).<sup>41</sup> Herein, 14 FET devices were adhered to the epoxy substrate using a thermo-curing process, and each FET sensor was aligned with the corresponding cell trap so that the cell presence could be detected (Fig. 4b).

### Fabrication of the FET sensor array and chip assembly

The 1.2 × 0.8 mm FET chip was fabricated by a molecular beam epitaxy process for the GaN and AlGaN layers, followed by plasma etching and metal deposition.<sup>36,41</sup> The 14 fabricated FET devices were then packaged as a sensor array onto an epoxy substrate. The packaging process included 1) aligning the FET chips upside-down onto a PDMS mold along the alignment marks, 2) pouring the epoxy resin (U-20F, *e.b.t.* liquid encapsulant, Taiwan) on the PDMS mold, and 3) curing the epoxy. Gold deposition was then undertaken to establish an electronic connection; photoresist was coated as the protection layer, and the open-gate area on the FET was defined accordingly. The transistor channel and gate

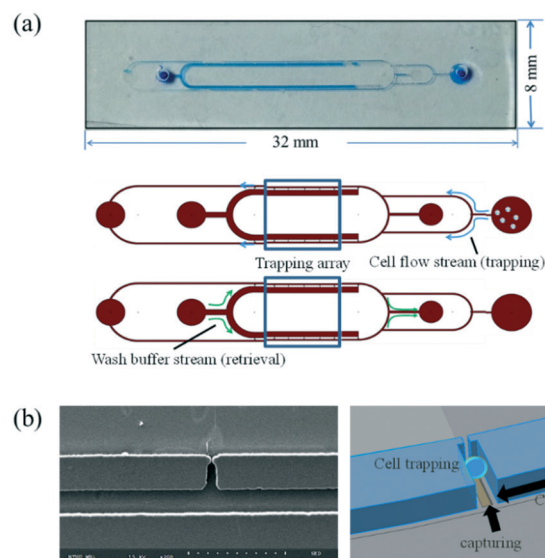


**Fig. 3** (a) The design of the microfluidic chip, including an image of the chip and a schematic illustration of the work flow for cell trapping and retrieval. (b) An SEM (SNE-3000M, SEC CO LTD, South Korea) image of the cell trap and a schematic illustration of the trapping process. The channel height was 30 μm.

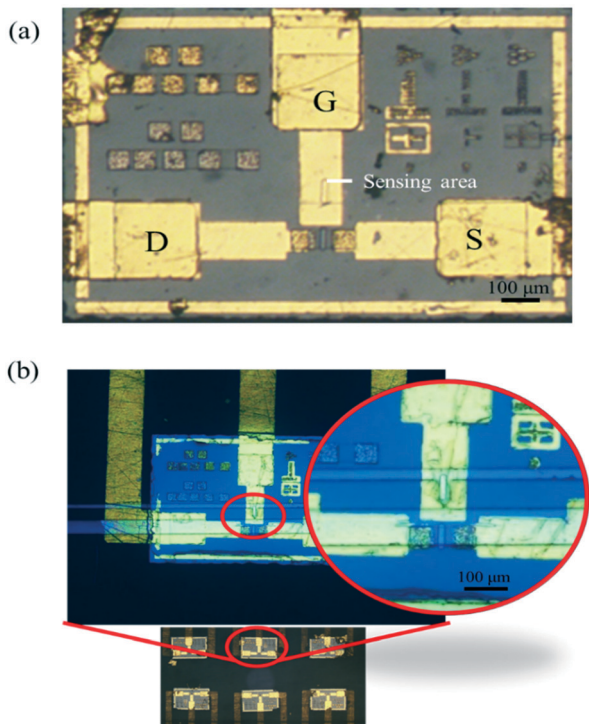


**Fig. 4** (a) An image of the epoxy substrate equipped with FET sensor arrays. D = drain, S = source, and G = gate. (b) The integration of the microfluidic channel and FET sensor arrays, which enabled cells to be trapped on the FET sensing area.

electrode opening areas were  $10 \times 60 \mu\text{m}^2$ , which were designed to match the size of the cells, to avoid overcrowding of cells and to provide an easy validation method *via* optical imaging to confirm the presence of cells. The distance between the transistor channel and gate electrode openings was maintained at  $65 \mu\text{m}$ . Afterwards, thin (thickness =  $30 \mu\text{m}$ ), laser-engraved, double-sided tape (Tesa, Germany) was used to bind the microfluidic chip to the FET array to prevent liquid leakage. Oxygen plasma treatment was applied to the PDMS microfluidic chip to tightly adhere it to the tape. The microfluidic chip and the FET substrate were bound carefully under an optical microscope such that the trapping chambers were precisely aligned with the open gates of each FET device. Herein, the integrated microfluidic device capable of trapping and detecting CTCs was assembled.

### Preparation of cancer cell lines

Colorectal cancer, among the most common malignancies, is characterized by high rates of metastasis.<sup>42</sup> In this work, the human colon cancer cell line HCT-8 was chosen as our target cell to model the CTC behavior in blood.<sup>43</sup> The cells were cultured in Roswell Park Memorial Institute (RPMI) media (Sigma-Aldrich, USA) with 10% fetal bovine serum (FBS, Life Technologies, USA) and incubated at  $37 \text{ }^\circ\text{C}$  and 5%  $\text{CO}_2$ . The cultured cells were then detached and suspended in either PBS (Merck, Germany) or RPMI media at a final concentration of  $10^4 \text{ ml}^{-1}$ . Additionally, the human ovarian cancer cell line

BG-1 was cultured in Dulbecco's minimum essential medium (Life Technologies, USA) with 10% FBS to serve as the non-target cells for the CTC selectivity test (described below). The cancer cells were spiked into human blood ( $10^3$  cells in 7.5 ml blood) to simulate a typical CTC sample from a patient<sup>44-46</sup> (IRB No. A-ER-103-063).

### Preparation of the HCT-8-specific aptamer-conjugated magnetic beads

Magnetic beads surface-coated with aptamers found previously to be specific to HCT-8 cells<sup>43</sup> were used herein to isolate CTCs from human blood. HCT-8-specific aptamers with a 5'-amine functional group were synthesized at a concentration of  $100 \mu\text{M}$  (Protech, Taiwan) and then conjugated to carboxylic acid-coated magnetic beads ( $4 \times 10^6$  beads per mL, Dynabeads® M-450 Epoxy, Invitrogen, USA) by carboxylation.<sup>43</sup> The sequence of the aptamer is shown as follows: 5'-TACAGCACCACAGACCATGGTTGTGTTTTTTTTTGTGTGGCTTCGTATGTTGTTGCGTGTGTTGTCTTCCTGCC-3', which was screened previously by our group.<sup>43</sup> The dissociation constant and cell capture percentage of this aptamer were previously found to be  $13.2 \pm 3.8 \text{ nM}$  and  $50.1 \pm 1.7\%$ , respectively, comparable to those of a commercial antibody.<sup>43</sup> The aptamer-conjugated magnetic beads were stored at  $4 \text{ }^\circ\text{C}$  in the dark prior to use.

### Immobilization of HCT-8 specific aptamers on a gold substrate

In order to capture the cancer cells on the FET gate (gold) surface, the HCT-8-specific aptamers ( $5 \mu\text{M}$ ,  $100 \mu\text{L}$ ) with thiol functionalization were immobilized on the open gold surface of the FET devices by addition of  $1 \mu\text{L}$  of  $100 \mu\text{M}$  Tris(2-carboxyethyl)phosphine hydrochloride (Sigma-Aldrich, USA), which acted to reduce the disulfide bonds and covalently bond the aptamers to the gold surface. After 24 h of incubation, the gold surface was immersed in PBS and stored at  $4 \text{ }^\circ\text{C}$  prior to use.

### Experimental procedures

RBC lysis and WBC depletion were first performed automatically on-chip as in our previous work with 7.5 ml of whole blood spiked with 1000 HCT-8 cells (Fig. 1).<sup>45</sup> Then, the cancer cells in the sample were captured by magnetic beads surface-coated with the HCT-8 specific aptamers. The bead-cell complexes were magnetically collected and injected into the integrated microfluidic chip *via* an air-pressure-driven flow control system (MFCS™-EZ, Fluigent, France). It is worth noting that the cancer cells may bypass the narrow neck of the cell trapping device if the provided pressure was higher than 4000 Pa (Fig. S2†). Therefore, a pressure of 3000 Pa was applied for all experiments. As a result of hydrodynamic trapping in the microfluidic channel, CTCs could be trapped in the desired region at an average flow rate of  $90 \mu\text{L min}^{-1}$  (above the FET's gate sensing area; *i.e.*, where the HCT-8 specific aptamers were immobilized). For the FET signal measurement, the bias was set at 2.5 V for the source-drain, and then a voltage

pulse was applied from 0 to 2 V over 50  $\mu\text{s}$  at the gate. The drain current change after increasing the gate bias was defined as the current gain, and the change in the current gain after capturing different numbers of CTCs was then measured. All signals from the FETs were recorded with a semiconductor analyzer (B1500A/B1530 Agilent, USA) on a probe station (IV curve & CV testing probe station, Sadhu Design, Taiwan).

When a gate bias  $V_g$  was applied, the capacitance across the solution  $C_s$  was established; an electric double layer was then formed at the interface. After target cells were captured on the gate surface, a serial capacitance  $C_{\text{cell}}$  (due to the capacitor-like nature of cell membranes) was maintained.<sup>47</sup> The current gain was determined by  $C_s$  and  $C_{\text{cell}}$ . Overall, the solution capacitance  $C_s$  was also affected by the number of cells captured on the FET; this accounts for why the FET sensor could be used for enumeration of target cancer cells.

## Results and discussion

### Hydrodynamic cell trapping

The mechanism underlying hydrodynamic trapping could be described by the concept of fluidic resistance.<sup>18</sup> In Fig. 5a,  $R_{h1}$  represents the flow resistance along the traps, which was designed to be smaller than the bypassing resistance,  $R_{h2}$ , when the traps were empty; therefore, the main stream could carry the cells into the trapping chambers such that the main stream could be switched into the bypassing route by increasing the resistance along the original path of  $R_{h1}$ . The following cells could be carried through the new path towards the subsequent traps. A numerical simulation was first used to explore the channel geometry and evaluate the velocity profile for desired fluidic resistance with COMSOL Multiphysics (COMSOL, USA) software. The velocity of the stream entering the first trap was found to be much greater than that of the other route (Fig. 5b),

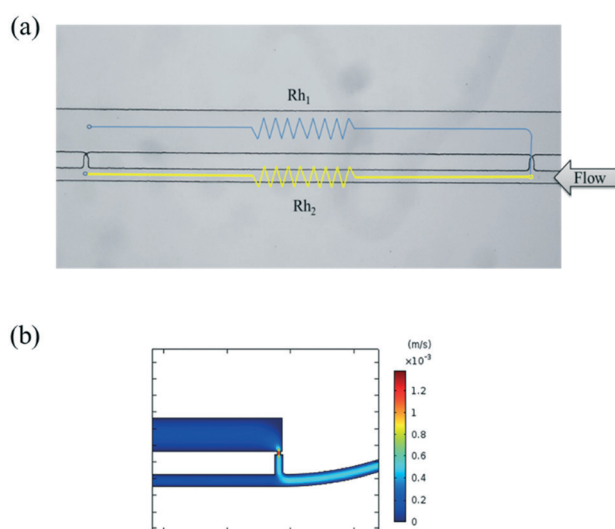


**Fig. 5** (a) The flow resistance  $R_{h1}$  was designed to be smaller than  $R_{h2}$ , such that cells could be trapped in the cell-trapping structures. (b) Numerically simulated velocity profile in the microfluidic chip revealing efficient cell-trapping.

indicating that the majority of the flow entered the trap. The numerical simulation showed that the designed dimensions established a fluidic resistance  $R_{h1}/R_{h2}$  ratio of 3, suitable for cell trapping<sup>20</sup> (Fig. S3<sup>†</sup>).

The cell trapping process on the microfluidic device was observed under an optical microscope (Fig. 6a). Cancer cells (diameter = 15  $\mu\text{m}$ ) were successfully guided into the chambers and then trapped by the chambers' narrow necks (width = 5  $\mu\text{m}$ ); then, the cells bound to the aptamers that had been previously immobilized on the surface of the FET. Note that cells could be retrieved and collected by applying a backward flow by using a micro-dispenser for subsequent applications (Fig. 6b).

### Cancer cell detection and enumeration by FET sensors

A FET sensor array was used to quantify the number of captured CTCs. The features of the AlGaIn/GaN HEMT sensor are summarized in Table S1.<sup>†</sup> For the electrical signal measurement, the change in the current between each FET's source and drain after gate bias application was defined as the "current gain." Typical drain current response and calculation of current gains are shown in Fig. S4.<sup>†</sup> After cells were injected through the inlet, different numbers of cells (typically 1–3) were trapped in the cell-trapping chamber precisely in the sensing area (Fig. 7a), and the changes in the current gain over 50  $\mu\text{s}$  for one, two, and three cells were measured to be  $9.3 \pm 0.9$ ,  $24.5 \pm 4.7$ , and  $38.7 \pm 4.5$   $\mu\text{A}$ , respectively; there was a positive correlation, then, between the current gain and the number of captured cells (Fig. 7b) such that the FET signals could serve as a proxy for cell counts in future studies. Furthermore, we have demonstrated that unbound cells or loosely bound cells (non-specific cells) did not affect the sensor signal, as only the strong electrostatic

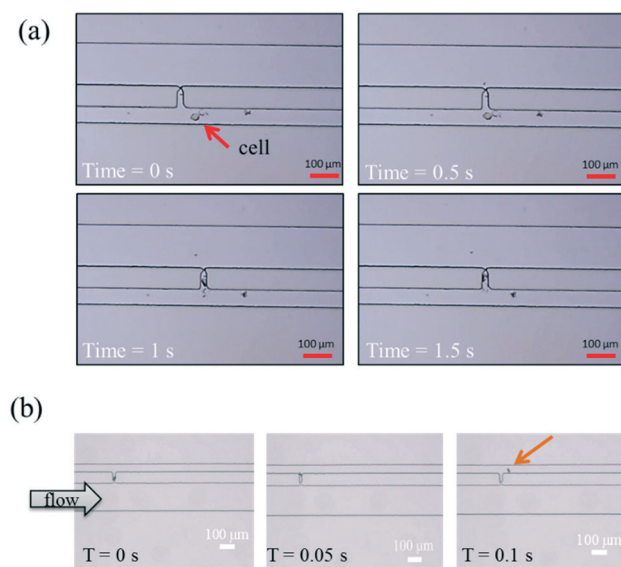


**Fig. 6** (a) Microscopy images depicting trapped cells. (b) Cell retrieval by applying a backwards flow.

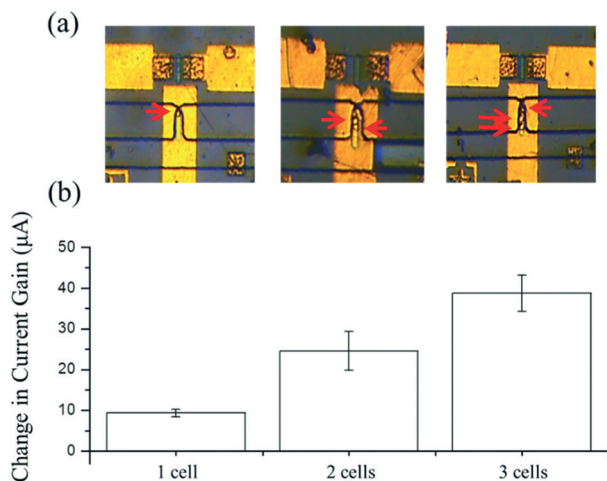


**Fig. 7** Current gain signals from FET devices for cancer cells captured by 1) microfluidic chambers and 2) aptamers immobilized on the surface of the gate areas. (a) Images of different numbers of cells captured on the sensors and (b) the corresponding changes in the current gain for each cell count.

interaction of the aptamer and target cell resulted in charge re-distribution within the double layer, which resulted in a change in the FET current signal.<sup>41,48</sup> Given the arrayed design and the fact that each trap could capture up to three cells, a maximum of 42 cancer cells could be captured and detected on the integrated microfluidic system. When compared with fluorescence measurements, this label-free detection method requires only a sample incubation period of 5 minutes, which is much faster when compared with hour-long sample incubation periods required for optical imaging techniques, which has shown great potential given its fast, simple, and label-free nature, as well as the accurate, quantitative results generated.<sup>34</sup>

### Selectivity tests

The selectivity of the FET sensor was further explored by utilizing two non-target cell lines, WBCs and BG-1 ovarian cancer cells, which were spiked into human blood and analyzed as described above for HCT-8 cells. Unlike the aforementioned positive relationship between the HCT-8 cell number and current gain, the current gain did not show an increasing trend for the non-target cells (Fig. 8), despite the fact that they were captured by the traps. This is likely attributed to the specificity of the aptamer since the binding force could mobilize only the target cells towards the electric double layer and onto the electrodes (thereby giving rise to measurable FET signal changes). Therefore, the integrated microfluidic system was proven to detect only target cell types. Since non-target cells were not detected, false-positive results are unlikely to be documented by this device. It is noted that the results shown in Fig. 7 and 8 were obtained from different FET devices. Therefore, the device-to-device variations (about 5–15%) in current gains, when no cell was

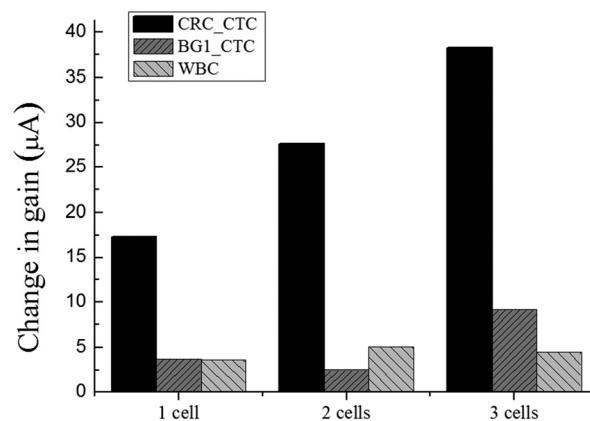


**Fig. 8** Changes in the current gain with different cell lines. The surfaces of the FET sensors were immobilized with HCT-8-specific aptamers; binding of HCT-8 cells only led to changes in current gain.

captured on the sensor, may result in differences in the calibration curves. For each FET sensor, a calibration curve for enumeration of cancer cells should be performed. If this technology will be transferred to industry in the future, it is feasible to minimize the sensor-to-sensor variations by a feasible quality control system.

## Conclusions

This study reported a new integrated microfluidic system for automatic detection and enumeration of CTCs. We demonstrated that the integration of hydrodynamic trapping devices on a microfluidic platform and FET sensor arrays could achieve cell trapping on the detection area and 0–3 cells on each sensor could be distinguished; herein the whole sensor array could capture and count 42 cancer cells in maximum. In addition, only the target cells bound to the specific aptamer on FET sensors could be detected. Given this, this design could prevent inevitable interference from other blood cells. In summary, an integrated microfluidic system equipped with FET sensor arrays, which could automatically capture and detect cancer cells, has been demonstrated. As such, it could serve as a useful tool for CTC detection and therefore, cancer diagnostics.

## Conflicts of interest

There are no conflicts to declare.

## Acknowledgements

The authors would like to acknowledge financial support from Taiwan's Ministry of Science and Technology (MOST 106-2119-M-007-008 and MOST 107-2314-B-007-005). Partial financial support from Taiwan's National Health Research Institute (NHRI-EX107-10728EI) and the Ministry of Education of Taiwan's Higher Education "Sprout" Project (Grant

No.107Q2713E1) is also greatly appreciated. The authors also thank Dr. Yan-Shen Shan at the National Cheng Kung University Hospital (Tainan, Taiwan) for providing human blood samples.

## Notes and references

- J. Ferlay, I. Soerjomataram, R. Dikshit, S. Eser, C. Mathers, M. Rebelo, D. M. Parkin, D. Forman and F. Bray, *Int. J. Cancer*, 2015, **136**, E359–386.
- S. Sleijfer, J.-W. Gratama, A. M. Sieuwerts, J. Kraan, J. W. M. Martens and J. A. Foekens, *Eur. J. Cancer*, 2007, **43**, 2645–2650.
- S. de Wit, G. van Dalum and L. W. M. M. Terstappen, *Scientifica*, 2014, **2014**, 11.
- M. Yu, S. Stott, M. Toner, S. Maheswaran and D. A. Haber, *J. Cell Biol.*, 2011, **192**, 373–382.
- M. S. Pepe, R. Etzioni, Z. Feng, J. D. Potter, M. L. Thompson, M. Thornquist, M. Winget and Y. Yasui, *J. Natl. Cancer Inst.*, 2001, **93**, 1054–1061.
- Q. Weiyi, Z. Yan and C. Weiqiang, *Small*, 2015, **11**, 3850–3872.
- S. Mocellin, U. Keilholz, C. R. Rossi and D. Nitti, *Trends Mol. Med.*, 2006, **12**, 130–139.
- M. Correnti and C. Raggi, *Oncotarget*, 2017, **8**, 7094–7115.
- E. Lagally, *Microfluidics and Nanotechnology Biosensing to the Single Molecule Limit*, CRC Press, 2017.
- P. Wang, L. Robert, J. Pelletier, W. L. Dang, F. Taddei, A. Wright and S. Jun, *Curr. Biol.*, 2010, **20**, 1099–1103.
- V. Chokkalingam, J. Tel, F. Wimmers, X. Liu, S. Semenov, J. Thiele, C. G. Figdor and W. T. Huck, *Lab Chip*, 2013, **13**, 4740–4744.
- J. Pelletier, K. Halvorsen, B.-Y. Ha, R. Paparcone, S. J. Sandler, C. L. Woldringh, W. P. Wong and S. Jun, *Proc. Natl. Acad. Sci. U. S. A.*, 2012, **109**, E2649–E2656.
- R. Riahi, P. Gogoi, S. Sepehri, Y. Zhou, I. Handique, J. Godsey and Y. X. Wang, *Int. J. Oncol.*, 2014, **44**, 1870–1878.
- C. D. Chin, V. Linder and S. K. Sia, *Lab Chip*, 2012, **12**, 2118–2134.
- N. Maluf and K. Williams, *An Introduction to Microelectromechanical Systems Engineering*, Artech House, Norwood, 2004.
- D. J. Beebe, G. A. Mensing and G. M. Walker, *Annu. Rev. Biomed. Eng.*, 2002, **4**, 261–286.
- L. R. Huang, E. C. Cox, R. H. Austin and J. C. Sturm, *Science*, 2004, **304**, 987–990.
- K. Louterback, J. D'Silva, L. Liu, A. Wu, R. H. Austin and J. C. Sturm, *AIP Adv.*, 2012, **2**, 42107.
- J. Zhou, C. Tu, Y. Liang, B. Huang, Y. Fang, X. Liang, I. Papautsky and X. Ye, *Sci. Rep.*, 2018, **8**, 9411.
- J. Nilsson, M. Evander, B. Hammarström and T. Laurell, *Anal. Chim. Acta*, 2009, **649**, 141–157.
- V. Narayanamurthy, S. Nagarajan, A. Y. F. Khan, F. Samsuri and T. M. Sridhar, *Anal. Methods*, 2017, **9**, 3751–3772.
- W.-H. Tan and S. Takeuchi, *Proc. Natl. Acad. Sci. U. S. A.*, 2007, **104**, 1146–1151.
- D.-H. Lee, X. Li, N. Ma, M. A. Digman and A. P. Lee, *Lab Chip*, 2018, **18**, 1349–1358.
- D. H. Lee, X. Li, A. Jiang and A. P. Lee, *Biomicrofluidics*, 2018, **12**, 054104.
- D. Di Carlo, N. Aghdam and L. P. Lee, *Anal. Chem.*, 2006, **78**, 4925–4930.
- A. Ahmad Khalili, M. Ahmad, M. Takeuchi, M. Nakajima, Y. Hasegawa and R. Mohamed Zulkifli, *Appl. Sci.*, 2016, **6**, 40.
- Y. D. Ma, K. Luo, W. H. Chang and G. B. Lee, *Lab Chip*, 2018, **18**, 296–303.
- S. Nagrath, L. V. Sequist, S. Maheswaran, D. W. Bell, D. Irimia, L. Ulkus, M. R. Smith, E. L. Kwak, S. Digumarthy, A. Muzikansky, P. Ryan, U. J. Balis, R. G. Tompkins, D. A. Haber and M. Toner, *Nature*, 2007, **450**, 1235–1239.
- C. Alix-Panabieres, H. Schwarzenbach and K. Pantel, *Annu. Rev. Med.*, 2012, **63**, 199–215.
- P. Went, M. Vasei, L. Bubendorf, L. Terracciano, L. Tornillo, U. Riede, J. Kononen, R. Simon, G. Sauter and P. A. Baeuerle, *Br. J. Cancer*, 2006, **94**, 128–135.
- K. Sefah, D. Shangguan, X. Xiong, M. B. O'Donoghue and W. Tan, *Nat. Protoc.*, 2010, **5**, 1169–1185.
- M. L. Kovarik, P. C. Gach, D. M. Ornoff, Y. Wang, J. Balowski, L. Farrag and N. L. Allbritton, *Anal. Chem.*, 2012, **84**, 516–540.
- M. Brischwein, E. R. Motrescu, E. Cabala, A. M. Otto, H. Grothe and B. Wolf, *Lab Chip*, 2003, **3**, 234–240.
- Y. L. Wang, B. H. Chu, K. H. Chen, C. Y. Chang, T. P. Lele, G. Papadi, J. K. Coleman, B. J. Sheppard, C. F. Dungen, S. J. Pearton, J. W. Johnson, P. Rajagopal, J. C. Roberts, E. L. Piner, K. J. Linthicum and F. Ren, *Appl. Phys. Lett.*, 2009, **94**.
- C. C. Huang, G. Y. Lee, J. I. Chyi, H. T. Cheng, C. P. Hsu, Y. R. Hsu, C. H. Hsu, Y. F. Huang, Y. C. Sun, C. C. Chen, S. S. Li, J. A. Yeh, D. J. Yao, F. Ren and Y. L. Wang, *Biosens. Bioelectron.*, 2013, **41**, 717–722.
- A. K. Pulikkathodi, I. Sarangadharan, Y. H. Chen, G. Y. Lee, J. I. Chyi, G. B. Lee and Y. L. Wang, *Lab Chip*, 2018, **18**, 1047–1056.
- D. Van Simaey, D. Lopez-Colon, K. Sefah, R. Sutphen, E. Jimenez and W. Tan, *PLoS One*, 2010, **5**, e13770.
- L. Y. Hung, C. H. Wang, C. Y. Fu, P. Gopinathan and G. B. Lee, *Lab Chip*, 2016, **16**, 2759–2774.
- Y. J. Che, H. W. Wu, L. Y. Hung, C. A. Liu, H. Y. Chang, K. Wang and G. B. Lee, *Biomicrofluidics*, 2015, **9**, 054121.
- M. A. Unger, H. P. Chou, T. Thorsen, A. Scherer and S. R. Quake, *Science*, 2000, **288**, 113–116.
- A. K. Pulikkathodi, I. Sarangadharan, Y.-H. Chen, G.-Y. Lee, J.-I. Chyi, G.-B. Lee and Y.-L. Wang, *ECS J. Solid State Sci. Technol.*, 2018, **7**, Q3001–Q3008.
- V. Patanaphan and O. M. Salazar, *South. Med. J.*, 1993, **86**, 38–41.
- L. Y. Hung, C. H. Wang, Y. J. Che, C. Y. Fu, H. Y. Chang, K. Wang and G. B. Lee, *Sci. Rep.*, 2015, **5**, 10326.
- S. Park, R. R. Ang, S. P. Duffy, J. Bazov, K. N. Chi, P. C. Black and H. S. Ma, *PLoS One*, 2014, **9**.

- 45 S. C. Tsai, L. Y. Hung and G. B. Lee, *Biomicrofluidics*, 2017, **11**, 034122.
- 46 Y. Zhang, X. F. Zhang, J. L. Zhang, S. Sun, L. L. Zheng, J. Li, S. X. Liu, G. D. Sui and Z. F. Yin, *Cancer Biol. Ther.*, 2016, **17**, 1177–1187.
- 47 T. P. Bothwell and H. P. Schwan, *Nature*, 1956, **178**, 265.
- 48 A. K. Pulikkathodi, I. Sarangadharan, C.-P. Hsu, Y.-H. Chen, L.-Y. Hung, G.-Y. Lee, J.-I. Chyi, G.-B. Lee and Y.-L. Wang, *Sens. Actuators, B*, 2018, **257**, 96–104.